

Superlattice gain in positive differential conductivity region

David O. Winge,^{1, a)} Martin Franckí,¹ and Andreas Wacker¹
Mathematical Physics, Lund University, Box 118, 22100 Lund, Sweden

(Dated: 6 January 2016)

We analyze theoretically a superlattice structure proposed by A. Andronov et al. [JETP Lett 102, 207 (2015)] to give gain in the Terahertz region. The existence of gain is confirmed but it is found to be strongly affected by elastic scattering, which limits the peak value. It is shown that the dephasing strongly modifies the nature of the relevant states, so that the common analysis based on Wannier Stark states is not reliable for a quantitative description of the gain in structures with extremely diagonal transitions.

Semiconductor superlattices¹ had always been considered as an interesting candidate for THz gain materials due to the Bloch gain², which was finally experimentally confirmed more than 30 years later³⁻⁵. However, this type of gain is intrinsically connected with the negative differential conductivity in the current-field relation, so that the formation of field domains⁶⁻⁹ strongly limits its observation and practical use. As an alternative, it was suggested¹⁰ that gain can be present in the positive differential conductivity region of superlattices where resonant tunneling over several barriers¹¹⁻¹³ is relevant. The idea is to operate the superlattice slightly below the tunneling resonance from the ground state of well μ to the excited state in the next-neighboring well $\mu + 2$ (see the inset of FIG. 1), which guarantees positive differential conductivity. At the same time, gain is suggested for the strongly diagonal transition to the excited state in the well $\mu + 3$, which is actually lower in energy than the ground state in well μ . More detailed experimental studies confirmed the suggested shape of the current-field relation, but were not conclusive with respect to THz gain¹⁴. Thus the question remains, whether this type of gain exists at all and whether it is strong enough to overcome losses. In order to address this question, we performed detailed simulations with our non-equilibrium Green's function (NEGF) simulation scheme¹⁵, which are reported here. We find that this particular gain mechanism exists, but that it is not particularly strong for the structure proposed. Testing different doping densities, we noticed that dephasing strongly reduces this type of gain. We show that this reduction can be explained by the nature of the eigenstates of the lesser Green's function, which represent better states to estimate gain than the conventional eigenstates of the Hamiltonian called Wannier-Stark (WS) states.

The NEGF model allows for a self-consistent evaluation of the transport with respect to both elastic and inelastic scattering as well as interactions with an electromagnetic field in semiconductor heterostructure devices¹⁵⁻¹⁹. It is particularly suitable for the study of semiconductor superlattices, as it contains simpler approaches, such as miniband transport¹, Wannier-Stark hopping^{20,21}, or sequential tunneling²² as limiting

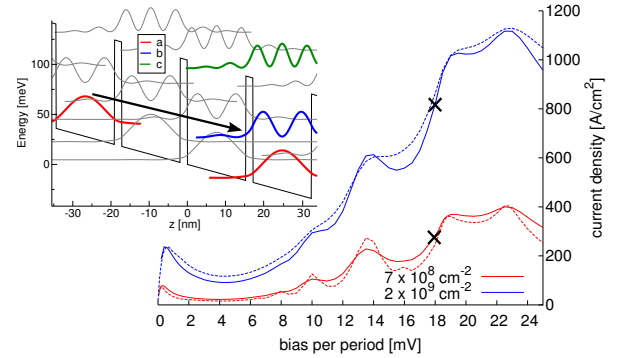


FIG. 1. Current-voltage characteristics for the samples studied. Simulations with modified scattering parameters are displayed as dashed lines. In the inset the configuration of the Wannier states at 18 mV is shown, marked by a cross in the main plot. The gain transition studied is indicated by an arrow.

cases²³.

In NEGF models, scattering is treated by self-energies that are evaluated self-consistently until convergence is reached. These objects are functions of both momentum and energy, but in our implementation they are effectively treated as only energy dependent, and evaluated at a representative set of momentum transfers for the scattering matrix elements¹⁵. This set is chosen by a typical energy transfer $E_{\text{typ}} = 3 \text{ meV} + 0.5k_B T$, fitted to give scattering matrix elements matching those calculated with thermalized subbands for other low doped heterostructures. While we consider this as reasonable for 77K, we apply also different values, in order to study increased or decreased scattering environments.

In this study all samples considered were assumed to be homogeneously doped. We also keep the lattice temperature fixed at 77 K, where we consider the model to be both robust and accurate.

FIG. 1 shows the calculated current voltage characteristics for the device of Ref. 14 (red solid line for a doping of $7 \times 10^8 / \text{cm}^2$ per period). The peak structure agrees reasonably well with the experimental data shown in FIG. 4 of Ref. 14. For comparison, the experimental shoulder at 19 mV per period, where the ground state is in resonance with the excited state of the 2nd nearest neighbor well, shows a current density of 450 A/cm^2 . In the following we focus on the operation point at 18

^{a)} Electronic mail: David.Winge@teorfys.lu.se

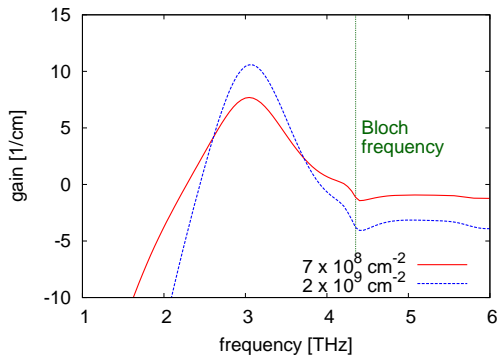


FIG. 2. Simulated gain for the two doping densities studied, both at a bias per period of 18 mV. There are small signatures of dispersive gain around the Bloch frequency and the structure is mainly transparent at higher frequencies.

mV per period, which is a stable operation point with positive differential conductivity. The inset in FIG. 1 shows the Wannier levels at this field. FIG. 2 shows the calculated gain (at weak cavity field). For the nominal structure (red solid line) it remains well below 10/cm, which is probably too small to overcome the total losses.

In the following we will employ a strict naming convention for the superlattice states (μ, ν) where μ will give the period index, with 0 for the central period, and ν for the state index. Here, Wannier states, are denoted by letters $\nu = a, b, c$ and Wannier Stark states (WS states, which are the eigenstates of the Hamiltonian) by roman numbers $\nu = i, ii, iii$. The tunneling resonance at the current peak at 19 mV per period is thus between Wannier levels (μ, a) and $(\mu + 2, b)$. At 18 mV per period the resonance between these levels is slightly detuned, so that the WS state (μ, i) is dominated by (μ, a) but has significant admixtures from $(\mu + 2, b)$ and $(\mu + 1, b)$. Similarly, the WS state $(\mu + 2, ii)$ is dominated by $(\mu + 2, b)$ with significant admixtures from (μ, a) , $(\mu + 1, b)$, and $(\mu + 3, b)$. These states are displayed in FIG. 3 (c) by full lines. The state (μ, i) is lower in energy than $(\mu + 2, ii)$ and has thus a significantly larger occupation.

Now the state $(\mu + 3, ii)$, which is equivalent to $(\mu + 2, ii)$, but shifted to the right and down in energy, is about 14.7 meV below the state (μ, i) . As both states extend over several periods they overlap significantly and furthermore there is inversion for the corresponding transition. We can attribute the gain shown in FIG. 2 to this transition, where a slight red shift can be explained by dispersive gain²⁴.

As an attempt to improve inversion and gain, the doping was increased to give a sheet density three times higher than the nominal sample. The result on current and gain is shown in FIG. 1 and FIG. 2, respectively. As expected the current density increases approximately by a factor three. However, the peak gain increases only slightly. Furthermore, in both samples there are small signatures of Bloch gain at around 4.2 THz and we also

Density [1/cm ²]	7×10^8		2×10^9	
Γ_1 (meV)	1.2	2.4	3.3	4.8
NEGF	18.8	7.69	10.6	-0.98
FGR(WS)	15.6	7.86	16.3	11.9
FGR($G^<$)	24.4	8.9	13.1	6.4

TABLE I. Estimated gain in units cm^{-1} from the gain transition using FGR with WS states and states from diagonalization of the lesser Green's function $G^<$, compared to the full NEGF calculations. The values are sorted by the lifetime broadening of the ground state Γ_1 .

observe that the high doped sample has more dark absorption at the frequencies far from the gain transition.

In the following, we want to study, why the increase of gain is limited, so that its practical use appears questionable. A naive guess, would be an increase of gain by a factor three just like the current. However, the inversion might not be proportional to the doping and the linewidth changes with doping. In order to study these effects, we use the standard estimate for the gain using Fermi's Golden Rule (FGR)

$$G(\omega) = \frac{\Delta E_{fi}}{\hbar} \frac{e^2 \Delta n_{fi} z_{fi}^2}{2n_r c \epsilon_0 d} \frac{\Gamma_w}{(\Delta E_{fi} - \hbar\omega)^2 + \Gamma_w^2/4} \quad (1)$$

where ΔE_{fi} is the energy difference between the initial and final states, Δn_{fi} is the inversion, z_{fi} the dipole matrix element, n_r is the refractive index and Γ_w is the full width half maximum of the gain peak. These variables can be extracted from the full NEGF model where we diagonalize the Hamiltonian including the real parts of the self-energies, on the diagonal in order to shift the single particle energy levels, to get the WS states. Here we approximate the linewidth as the sum of the lifetimes of the two states involved, $\Gamma_w = \gamma_f + \gamma_i$.

The result of this estimate is shown in TAB. I for a set of different model systems. The two middle columns of TAB. I refer to our standard simulation parameters as used in FIGS. 1-2. Furthermore, we also performed simulations by changing E_{typ} . The data in the left-most/right-most column are for decreased/increased scattering compared to their neighboring column. This is reflected by the respective width of the ground state Γ_1 , which is extracted from the NEGF calculation. The current simulations for these parameters are shown alongside the standard ones in FIG. 1 as dashed lines. It is clear that the effect on the current is limited, it merely broadens/sharpens the tunneling resonances for decreased/increased scattering.

Let us first consider the estimate from FGR (1) with the common WS states in TAB. I. Here we find, that the peak gain follows essentially the doping density divided by Γ_1 , which shows that the inversion is essentially proportional to doping, and all other ingredients, except for the broadening, are constant. In contrast, the NEGF calculation shows a much stronger decrease of gain with Γ_1 . While a part of the differences may be attributed

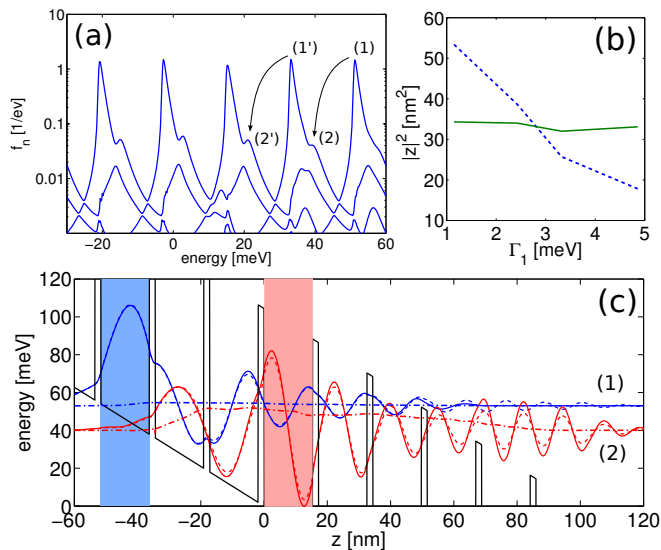


FIG. 3. (a) Eigenvalues $f_n(E)$ of the lesser Green's function $(2\pi i) G_{\alpha\beta}^<(\mathbf{k} = 0, E)$ at each energy point. (b) Modulus square of the dipole matrix elements against the energy broadening of the ground state. The eigenstates of the density matrix (dashed blue) is strongly dependent on scattering as opposed to Wannier-Stark states (solid green). (c) Real part of the eigenstates (dashed) corresponding to the eigenvalues indicated in (a). The imaginary part is visualized by plotting the current carrying combination²⁵ $\Re\{-i\phi^* d\phi/dz/m^*\}$ (dotted-dashed) for both eigenstates. These can be seen, especially for state (2), to extend over several periods. For easy comparison we plot also the Wannier-Stark states (μ, i) (blue solid line) and $(\mu + 3, ii)$ (blue)(red solid line). The well where each wavefunction has its origin is shaded as guidance.

to the widening of other absorbing transitions, the large extent is stunning.

To understand this discrepancy we analyze instead the eigenstates of lesser Green's function $G_{\alpha\beta}^<(\mathbf{k}, E)$ (which can be viewed as the energetically resolved density matrix) following Ref. 25. The eigenvalues for the nominal case with $\Gamma_1 = 2.4$ are plotted in FIG. 3 (a) for $\mathbf{k} = 0$. The eigenvalues show where the states are located in energy, and they also visualize the inversion at an energy of 12 meV (indicated by arrows), corresponding to 3 THz. As the eigenvalues are sorted by size in the diagonalization process, we see anti-crossings where the different eigenstates passes each other, so that the state at the eigenvalue indicated by (2) is not the same as the one at (1) since they are separated by at least one anti-crossing.

At the eigenvalue peaks (1) and (2) we plot the corresponding eigenstates in FIG. 3 (c) together with the WS states. From this plot it is possible to see that compared to the WS states, the eigenstates of the Green's function are slightly more delocalized for these sample parameters. For example state $(\mu, 1)$ extends much further out to the neighboring periods than (μ, i) , allowing for a larger overlap and thus a higher dipole matrix element with $(\mu + 3, 2)$ or $(\mu + 3, ii)$. In FIG. 3 (b) the

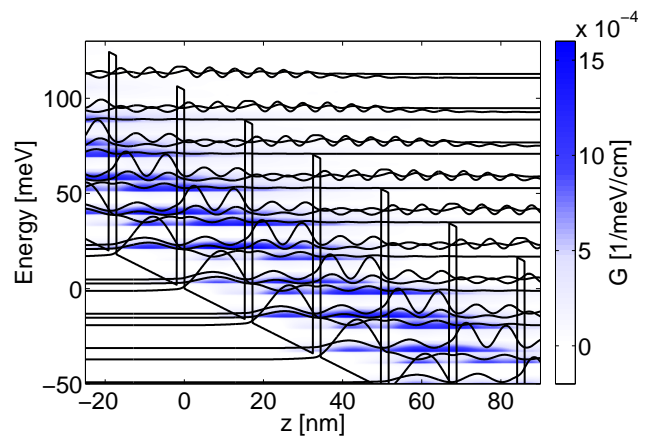


FIG. 4. Gain at 3 THz resolved in energy and space for the nominal case with $\Gamma_1 = 2.4$ meV. The coherence giving rise to the gain extends over several periods. The bias is 18 mV per period.

modulus square of the dipole matrix elements are plotted versus the width of the ground state. The WS states show small variations due to meanfield and renormalization due to scattering, but are otherwise constant. In contrast, the dipole matrix elements, calculated by the eigenstates of the Green's function provide a strong decrease with increasing scattering. These dipole matrix elements can be applied in FGR (1), and the results are given in the lowest line of TAB. I. They actually follow the trend of the full calculation, which demonstrates the relevance of these eigenstates. The result by FGR naturally overestimates the gain slightly, as we consider the gain from only one transition while all other (mostly absorbing) transitions are neglected, while they are fully taken into account in the NEGF model.

The strong Γ -dependence of the eigenstates of the lesser Green's function is reflected by dephasing, which affects the coherence length. In this particular situation, the gain is highly diagonal and is thus dependent on these spatial coherences. This is further demonstrated in FIG. 4, where the gain stripes extend over more than 50 nm. As impurity scattering is strongly dependent on temperature due to screening, we expect higher gain at lower temperatures, which might be sufficient for lasing in the higher doped structure. Preliminary simulations with the model predict, that a lattice temperature below 50 K results in gain over 20/cm for our standard parameters²⁶.

As the optimization using carrier densities did not yield any spectacular increase in performance, we studied in addition, whether gain can be enhanced by adjusting the well width. In FIG. 5 we display results for samples named *wide/ narrow* where the width of the quantum well was increased/decreased by 4 monolayers, respectively, while the sheet doping density was kept constant at $7 \times 10^8/\text{cm}^2$. The data shows that the peak gain hardly depends on the well width, which merely causes a shift

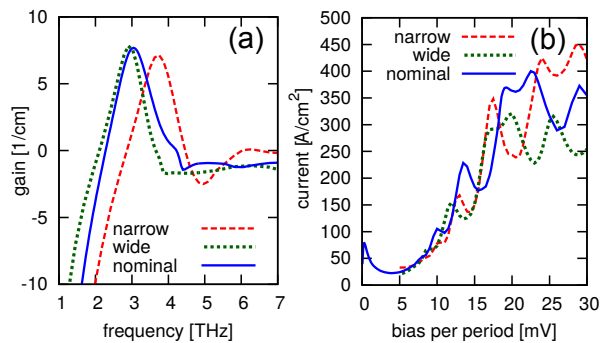


FIG. 5. (a) Gain and current (b) for standard scattering parameters for the two altered structures as well as the nominal sample from Ref. 14. The operating bias per period was 16 mV and 23 mV for the *wide* and *narrow* structure, respectively.

in the peak frequency.

In conclusion, we have shown that the NEGF model predicts gain in the structure from Ref. 14 for a lattice temperature of 77 K, which is however relatively small. We did not find significant improvements by increasing doping or changing the well width. However, improved screening at lower temperatures may allow for observing laser emission.

For this highly diagonal transition, the gain is strongly dependent on the scattering. This can be demonstrated by the eigenstates of the lesser Green's function, which essentially differ from the WS states in this case. We demonstrated that these unconventional states are more appropriate to calculate the z-matrix elements for a quantitative description of gain by Fermi's golden rule.

ACKNOWLEDGMENTS

We thank A. Andronov and J. Faist for helpful discussions and the Swedish Research Council for financial

support.

- ¹L. Esaki and R. Tsu, IBM J. Res. Dev. **14**, 61 (1970).
- ²S. A. Ktitorov, G. S. Simin, and V. Y. Sindalovskii, Sov. Phys.-Sol. State **13**, 1872 (1972), [Fizika Tverdogo Tela **13**, 2230 (1971)].
- ³Y. Shimada, K. Hirakawa, M. Odnobliudov, and K. A. Chao, Phys. Rev. Lett. **90**, 046806 (2003).
- ⁴P. G. Savvidis, B. Kolasa, G. Lee, and S. J. Allen, Phys. Rev. Lett. **92**, 196802 (2004).
- ⁵N. Sekine and K. Hirakawa, Phys. Rev. Lett. **94**, 057408 (2005).
- ⁶L. Esaki and L. L. Chang, Phys. Rev. Lett. **33**, 495 (1974).
- ⁷H. T. Grahn, ed., *Semiconductor Superlattices, Growth and Electronic Properties* (World Scientific, Singapore, 1995).
- ⁸A. Wacker, Phys. Rep. **357**, 1 (2002).
- ⁹L. L. Bonilla and H. T. Grahn, Reports on Progress in Physics **68**, 577 (2005).
- ¹⁰A. A. Andronov, E. P. Dodin, D. I. Zinchenko, and Y. N. Nozdrin, Journal of Physics: Conference Series **193**, 012079 (2009).
- ¹¹H. Schneider, H. T. Grahn, K. v. Klitzing, and K. Ploog, Phys. Rev. Lett. **65**, 2720 (1990).
- ¹²A. Sibille, J. F. Palmier, and F. Laruelle, Phys. Rev. Lett. **80**, 4506 (1998).
- ¹³M. Helm, W. Hilber, G. Strasser, R. De Meester, F. M. Peeters, and A. Wacker, Phys. Rev. Lett. **82**, 3120 (1999).
- ¹⁴A. Andronov, E. Dodin, D. Zinchenko, Y. Nozdrin, M. Ladugin, A. Marmalyuk, A. Padalitsa, V. Belyakov, I. Ladenkov, and A. Fefelov, JETP Lett+ **102**, 207 (2015).
- ¹⁵A. Wacker, M. Lindskog, and D. Winge, Sel. Top. in Quantum Electron., IEEE Journal of **19**, 1200611 (2013).
- ¹⁶T. Schmielau and M. Pereira, Appl. Phys. Lett. **95**, 231111 (2009).
- ¹⁷T. Kubis, C. Yeh, P. Vogl, A. Benz, G. Fasching, and C. Deutsch, Phys. Rev. B **79**, 195323 (2009).
- ¹⁸G. Haldas and, A. Kolek, and I. Tralle, Quantum Electron., IEEE Journal of **47**, 878 (2011).
- ¹⁹T. Grange, Phys. Rev. B **92**, 241306 (2015).
- ²⁰R. Tsu and G. Döhler, Phys. Rev. B **12**, 680 (1975).
- ²¹D. Calecki, J. F. Palmier, and A. Chomette, J. Phys. C: Solid State Phys. **17**, 5017 (1984).
- ²²R. F. Kazarinov and R. A. Suris, Sov. Phys. Semicond. **5**, 707 (1971).
- ²³A. Wacker and A.-P. Jauho, Phys. Rev. Lett. **80**, 369 (1998).
- ²⁴R. Terazzi, T. Gresch, M. Giovannini, N. Hoyler, N. Sekine, and J. Faist, Nature Physics **3**, 329 (2007).
- ²⁵S.-C. Lee, F. Banit, M. Woerner, and A. Wacker, Phys. Rev. B **73**, 245320 (2006).
- ²⁶However, we refrain from making a definite statement, as we encountered inaccuracies for different samples at such low temperatures.